Regular Article

Droplet on a regularly patterned solid. Wenzel's regime and meso-scale roughness

Waldemar Nowicki[a], Bartłomiej Gątarski[b], and Marcin Dokowicz[c]

Faculty of Chemistry, Adam Mickiewicz University in Poznań, Umultowska 89b, 61-614 Poznań, Poland

© The Author(s) 2015. This article is published with open access at Springerlink.com

Abstract. The applicability of Wenzel's equation to describe a liquid droplet settled on the solid surface regularly patterned with rectangular prisms was examined by means of simulations of the droplet/surface system morphology and energetics. The droplet deposited on the meso-scale surface roughness (*i.e.* the droplet size was larger than the size of heterogeneities by about an order of magnitude) was considered. Several different approaches to the estimation of the contact angle were employed. The discrepancies between the results of simulated experimental measurements and the predictions based on the Wenzel equation were analyzed and discussed. The influence of three-phase contact line effects on the droplet morphology and the existence of metastable states was shown.

1 Introduction

Wetting phenomena have been the subject of numerous experimental and theoretical studies since their understanding is related to many significant technological and industrial applications, including lubrication, coating, printing, waste water treatment, mineral processing, and microfluidics [1–4]. A widely used approach to characterization of wetting properties of surfaces involves the measurement of contact angles (CAs). For the ideal, namely perfectly smooth and chemically homogeneous solid surfaces, the relation between CA and the surface free energy has been developed by Thomas Young [5]. However, most of the natural or fabricated surfaces are geometrically or chemically heterogeneous. In extreme cases, in which the liquid completely penetrates into all cavities producing homogenous liquid-solid interface, or in which some gas bubbles remain entrapped underneath a droplet, the morphology of a liquid droplet settled on a geometrically heterogeneous (rough) surface can be described in categories of the Wenzel regime [6] or the Cassie regime [7], respectively.

In the Wenzel regime, the CA measured on the rough surface (the Wenzel CA, θ_W) can be predicted from the equation [9]

$$\cos(\theta_W) = \frac{S}{S_=} \cos(\theta^*) = f \cos(\theta^*), \qquad (1)$$

in which parameters S and $S_=$ stand for the actual area of the solid surface and the area of its projection on the plane parallel to it, θ^* is the CA characterizing the solid material of ideally smooth surface (Young CA [10]) and f represents the so-called surface roughness parameter (or roughness ratio) [11,12].

Equation (1) holds when a droplet takes shape of a spherical cap according to the Plateau law [6,13–15] and the droplet size is infinitely larger than the scale of the roughness [16]. The Wenzel law correctly predicts the trend of the apparent (*i.e.*, experimentally measured) CA with increasing roughness of hydrophilic or hydrophobic surfaces when the droplet is sufficiently large compared with the scale of roughness [17]. But, even when the relative size of heterogeneities is very small, the droplet assumes an asymmetric irregular shape with the corrugated three-phase contact line (triple line) [13,14,18–20], especially for the inhomogeneities represented by linear grooves, where the droplet behavior in parallel and perpendicular directions to the grooves is different [21]. However, if the size of inhomogeneities remains small as compared to the droplet size (micro-roughness), the corrugation of the triple line due to imperfections of the solid surface does not produce a significant discrepancy between measured CAs and those predicted by the Wenzel equation [14–17,22–25]. On the other hand, with a decrease in the droplet size relative to the size of surface roughness features, the predictive applicability of the Wenzel equation has often been observed to fail [26,27].

For a small droplet the contribution of interactions at the triple line becomes significant enough to affect its

---

[a] e-mail: gwnow@amu.edu.pl
[b] e-mail: gatar@interia.pl
[c] e-mail: dokowicz@amu.edu.pl

wetting behavior [28,29]. The critical importance of the triple line in the wetting behavior was shown by Gao and McCarthy [23], who found experimentally that CA of a droplet is defined solely by the triple line, while the roughness beneath the droplet is irrelevant. However, there are still many controversies regarding the conclusion of Gao and McCarthy. The extensive reviews on this topic have been published recently [30,31].

A mechanism which is most often proposed as responsible for the discrepancy between CAs measured on rough surfaces and those predicted from the Wenzel equation is the apparent pinning of the triple line on surface defects, such as the edges of asperities [14]. The results of some studies indicate the existence of factors affecting the CA on rough surfaces different from the pinning of the triple line to sharp edges of surface structure features. For instance, Promraksa *et al.* [8,32] studied the droplet behavior on a surface represented by a square array of cosine wave-like pattern, that is on the surface whose roughness was classified by de Gennes *et al.* [10] as "soft" (*i.e.*, the surface whose shape can be described in terms of the function that is continuously differentiable) and demonstrated, both experimentally and on the basis of simulation methods, that the wetting phenomena occurring in the studied system cannot be described in categories based on the averaging of free interfacial energies over all geometric irregularities (in Wenzel's regime) nor on energetic inhomogeneities (in the Cassie regime) but should be related to the successive wetting transition from the Wenzel to the Cassie regime. The mixed wetting state (*i.e.* wetting partly in Wenzel's and partly in Cassie's regimes) have been also reported by Miwa *et al.* [33] and Marmur [34]. Additional discrepancy between CAS measured experimentally and predicted by Wenzel's law can be caused by the effect of impregnation of the solid material [35].

Deformation of the triple line caused by the pinning has been extensively studied both theoretically [25,36–38] and experimentally [15,39,40]. It was found, that droplets are often trapped in metastable states [14] separated by free energy barriers [41–43]. Pinning effect may cause a strong wetting hysteresis [44] and wetting anisotropy [45]. The droplet on anisotropic structured surfaces exhibits different CAs along the directions parallel and perpendicular to the surface features [46]; a difference of up to 25% in CA measured for the same droplet was observed [47]. The significance of the triple-line influence on the apparent CA depends on the degree of non-uniformity of the surface roughness; the effect matters much for strongly non-uniform roughness [48].

The corrugation of the triple line due to pinning effects depends rather on the size of surface inhomogeneities than on the surface roughness (defined by the parameter f), thus the inhomogeneity size is an important factor determining the departure of CAs from Wenzel predictions. Three different ranges of the surface roughness scale with regard to the droplet size can be distinguished: macro-, meso- and micro-scale roughness. In the case of macro-roughness (*i.e.*, if the size of a heterogeneity is comparable to the size of the droplet), the droplet can spon-

taneously change its position and shift to a fragment of the surface which is energetically more favorable and then its morphology and CA can be described by i) the Young equation taking into account the slopes and the area of the wetted planes and ii) by the equations/inequalities taking into account the effects at the sharp edges of inhomogeneities (pinning or spreading effects [49,50]). Thus, in the case of macro-scale roughness a good estimation of the CA can be obtained from the Young equation. For micro-scale roughness, such an estimation is given by the Wenzel equation (in the Wenzel regime where liquid penetrates the surface texture). In the case of both, macro- and micro-scale roughness the estimations of CA are based on its interpretation in terms of interfacial free energy. In the intermediate range of the roughness scale, the morphology of a droplet is mostly determined not by the interfacial effects but by phenomena occurring at the triple line, as numerous recent studies have indicated.

In this paper a correlation between the morphology of the droplet settled on a surface with a meso-scale roughness (represented by a regular pattern of geometric forms having sharp edges and whose sizes were from a few to about 20 times smaller than the size of the droplet) and the interfacial free energy as well as the triple-line effects was examined through computer simulation. To this end, the values of CA were estimated employing several methods differing in the way this quantity is assessed and compared with the CAs calculated on the basis of interfacial thermodynamics, assumed as reference values.

The CA estimations were obtained by minimization of the interfacial free energy of the system. In order to characterize the dispersion of CAs found by means of standard experimental methods and caused by different initial states of the deposited droplet, distributions and mean values of CAs computed series of independent simulations were carefully analyzed.

2 Methodology

The system under consideration consisted of a droplet settled on the solid surface decorated with a regular pattern of geometrical forms of a shape close to rectangular prisms of a square base with a constant height and a variable length of the edge of the base. The details of the solid-surface shape were defined by the equation

$$z = I\left(\frac{x}{L} \bmod 2 - \frac{x}{L} \bmod 1 + \frac{y}{L} \bmod 2 - \frac{y}{L} \bmod 1\right),$$

(2)

where x, y and z are the Cartesian coordinates of the surface points, L is the base edge length (different in each simulation series) and I the height of surface roughness elements (or, in other words, the amplitude of surface roughness). In simulations, the actual angles α between the side and top walls of geometrical forms modeling the surface defects were slightly greater than those following from eq. (2) and were equal to $(105 \pm 3)°$; thus these surface structure elements had the shape of squared frusta.
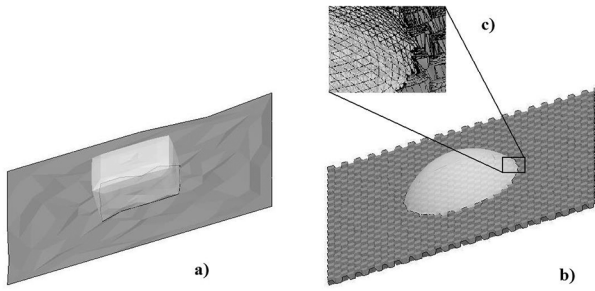
Fig. 1. The droplet settled onto solid surface a) the initial mesh, b) the mesh after several iterations (there is seen much better reproduction of the details of the surface structure as compared with the starting situation), c) the schematic view of the triple line in the course of simulation. The black color indicates triangles chosen for the calculation of θ_T ($A = 1.5$, $I/V^{1/3} = 0.175$, $L/V^{1/3} = 0.263$, $T/V^{1/3} = 5.8 \cdot 10^{-3}$, $\theta^* = 60°$).

Fig. 2. Modes of deposition of the droplet on the solid surface characterized by different values of the parameter A: (a) $A < 1$, (b) $A > 1$.

The simulations of behavior of the droplet deposited onto the analyzed surface was performed using the public-domain program Surface Evolver [51,52]. In the course of simulations, the morphology of the droplet at a stationary state was obtained by minimizing the interfacial energies. The liquid and solid surfaces were represented by a mesh of small triangles spanning the nodes. Mechanically stable interface configurations were obtained by minimizing the sum of interfacial energies being functions of the coordinates of the nodes. Furthermore, a fixed liquid volume was constant during energy minimization, representing an integral constraint to the shape of the liquid surface. Nodes belonging to the triple line were subject to a local constraint because their motion was restricted to the boundary determined by surface equation (2). Minimization steps included a combination of conjugate gradient descent steps and refinements of triangulated surfaces made to portray the details of solid surface. The simulation started with the solid surface practically free from roughness details defined by eq. (2), as shown in fig. 1a. In initial stages of simulations, the edge of the evolving droplet, representing the triple line, could freely move on the solid surface.

In the course of the simulations and refinement of the surface shape, the number of nodes increased, so also increased the accuracy of mapping of the surface eq. (2) (see fig. 1b), which led to the appearance of sharp edges hindering the free movement of the triple line.

As in the system analyzed the geometric parameters of the droplet morphology and the droplet energy were expected to be dependent on the initial position of the droplet with respect to the solid, the studies were performed assuming random initial droplet positions and different scenarios of reaching the stationary state by the droplet. These scenarios were realized by a chaotic shift (fluctuation) of the nodes, described by the vector produced by a generator of pseudo-random numbers from the range $[0, T)$, where T is the maximum amplitude of fluctuations. The random modifications of the droplet and solid surface were applied to mimic the real procedure of
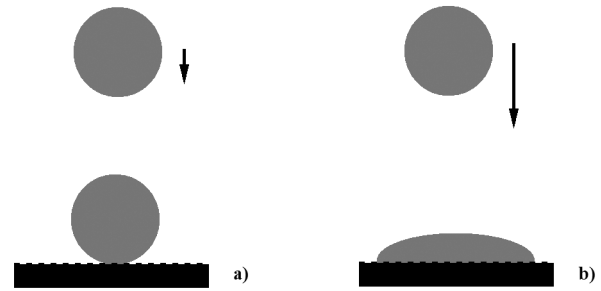
droplet deposition, which is practically unrepeatable (it is impossible to deposit a droplet in the same exact spot and thus, the initial droplet positions in repeated trials are determined by somewhat different locations of the triple line on the surface). The independent simulations gave droplet morphologies differing in details and different values of the final parameters describing the geometry and energy of the system. The final position of the droplet on the solid surface was stable and did not undergo measurable changes, as it was checked in the independent simulations including additional iterative steps.

The shape of the initial lump reproducing the droplet (rectangular cuboid of square base) from which the simulations started, was determined by an index A (termed in this paper as the index of initial droplet flattening), defined as the ratio of the length of the base edge to the height of the cuboid. In the model this index reflected the mode of droplet deposition on the solid surface: a small value of A corresponded to a delicate deposition with no deformation of the droplet (its shape was close to a sphere), while a high value of A corresponded to a high impact deposition accompanied by flattening of the droplet [53,54], as shown schematically in fig. 2. The simulations were performed for different values of A and T.

At the end of simulations, some parameters characterizing the equilibrium morphology were calculated: the internal Surface Evolver variables like the internal pressure, some geometrical features of the droplet and the total free energy of the system including all interfacial energies. Additional calculations involving the solution of implicit eqs. (10) and (14) were performed by numerical methods in the SciLab package [55].

For convenience, in all simulations the gravitational effects were neglected. Also, the line tension was not incorporated in the model. Moreover, it was assumed that in all cases considered, the surface wetting was realized in the Wenzel regime, that is, there were no unwetted points on the solid surface within the circumference marking the droplet contact with the surface [3].

All types of CAs considered in this study (and described in detail in sects. 3.1–3.5) were obtained from 4000 independent simulations. The mean values of CAs were calculated as averages of cosine of appropriate angles
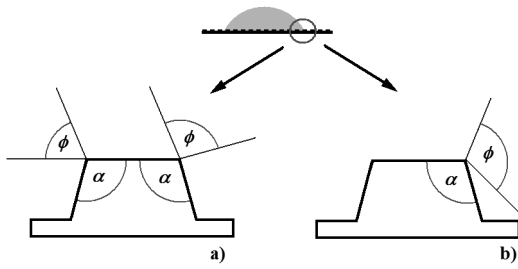
Fig. 3. Schematic presentation of the limiting values of the pinning angles ϕ for a) $\theta^* = 60°$ and b) $\theta^* = 120°$. Since the figure refers to the right side of the droplet, the left edges of a rectangular prism are internal whereas the right edges are external with regard to the droplet centre.

achieved on the basis of the mean values of the parameters describing the surface and energy of the droplet, according to the equations given in sect. 4.

Simulations were performed for two values of θ^* equal to 60° and 120°.

The assumed values of θ^*, together with the values of α, determined the behavior of the droplet in the course of simulation. And thus, since these values did not respect the following condition (known as the Concus-Finn condition [49]):

$$2\theta^* + \alpha \leq 180°, \tag{3}$$

there was no unlimited spreading of the droplet along interior edges of the surface structure.

On the other hand, another criterion, given by the following inequality [6,30]:

$$180° - 2\alpha < 0, \tag{4}$$

was fulfilled, which implied that the liquid could cross the concave bottom edges and fill up the cavities in the solid-surface structure.

The presence of sharp edges on the surface structure features can cause the pinning of the triple line. The pinning appears if the angle between the free liquid surface and the wall of the surface structure element, hereafter referred as the pinning angle, satisfies the so-called canthotaxis condition expressed by [50]

$$\theta^* \leq \phi \leq \theta^* + \alpha, \tag{5}$$

where ϕ denotes the pinning angle which can take any value from the range limited by the above inequality. If condition (5) is satisfied, the Young equation no longer works; the slope of the free surface of the droplet will be defined rather by ϕ than by θ^*.

For the assumed values of θ^*, the values of ϕ must come from the ranges (60°, 165°) and (120°, 225°), respectively, which means that for both studied values of θ^*, the pinning effect can be expected at both the internal and external edges of surface features (see fig. 3 for the explanation), and the actual pinning angle measured with respect to the plane parallel to the solid can vary in the following ranges:

1) $\theta^* = 60° \Rightarrow \varphi \in (0°, 60°)$ for the internal edge and $\varphi \in (60°, 165°)$ for the external edge,

2) $\theta^* = 120° \Rightarrow \varphi \in (120°, 225°)$ for the external edge.

3 Estimations of apparent CA

In this section different approaches to the evaluation of CA from the simulation results, used in the study, are presented.

3.1 CA from the surface roughness parameter

The theoretical value of Wenzel CA, θ_W, was calculated from eq. (1) on the basis of the surface roughness parameter f, which was found from the value of surface area of the solid S obtained from simulations. The mean Wenzel CA, $\langle \theta_E \rangle$ was found from

$$\cos(\langle \theta_W \rangle) = \left\langle \frac{S}{S_=} \right\rangle \cos(\theta^*), \tag{6}$$

where $S_=$ is the area of the projection of the solid surface onto the planar parallel surface.

This estimation of CA is based only on the properties of the solid surface applied.

3.2 CA from the solid/liquid interface area

Similarly as above, the CA was calculated from eq. (1), but instead of the surface roughness parameter, the actual area of the solid surface wetted by the droplet, S_d, obtained by the numerical minimization of the interfacial energies of the system, was used. The CA calculated in this way was denoted as θ_E. The mean value of this angle, $\langle \theta_E \rangle$, was calculated from the equation

$$\cos(\langle \theta_E \rangle) = \left\langle \frac{S_d}{S_{d=}} \right\rangle \cos(\theta^*), \tag{7}$$

where $S_{d=}$ stands for the area of projection of S_d onto the plane parallel to surface. The CA found in this way takes into account the pinning effect of the triple line at surface edges.

3.3 CA from the tangent angle at the triple line

The most widely used technique of CA measurement is a direct measurement of the tangent angle at the three-phase contact point on a sessile drop profile [2]. In this study, the values of this angle denoted as θ_T were calculated on the basis of the inclination of all mesh triangles representing the free liquid surface and being in contact with the triple line to the plane parallel to the solid surface from eq. (8a), while the mean values $\langle \theta_T \rangle$ were then obtained from eq. (8b):
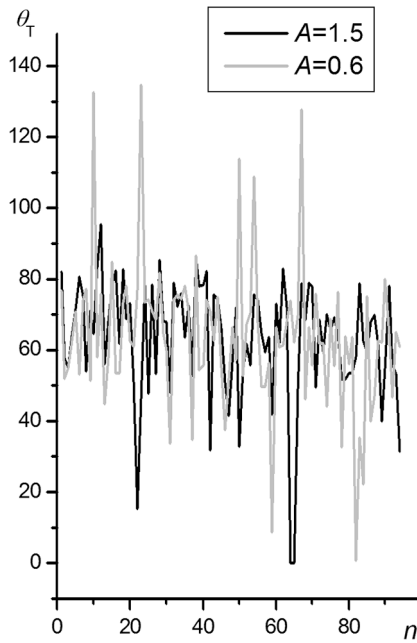
$$\theta_T = \arccos\left(\frac{z}{S_T}\right) \tag{8a}$$

Fig. 4. The values of θ_{T} measured along the droplet contour (n is the number of subsequent triangles) at two different values of A (indicated in the figure legend); and $\theta^* = 60°$, $I/V^{1/3} = 0.175$, $L/V^{1/3} = 0.263$, $T/V^{1/3} = 5.8 \cdot 10^{-3}$.

and

$$\langle\theta_{\mathrm{T}}\rangle = \arccos\left(\left\langle\frac{z}{S_{\mathrm{T}}}\right\rangle\right), \tag{8b}$$

where z and S_{T} denote correspondingly the vertical coordinate and the length of the normal vector of a triangle. The triangles whose slopes were used for evaluation of θ_{T} are indicated in fig. 1c.

The averaging of θ_{T}, discussed later on, was performed for the entire perimeter of the droplet obtained in a single simulation and for the all series of simulations. The θ_{T} values obtained from a single simulation revealed a considerable variation and deviated from Wenzel's law prediction. They oscillated in a very broad range, assuming the values consistent with the predictions based of the ranges of the pinning angle ϕ (inequality (5)), as shown in fig. 4.

3.4 CA from the droplet shape

The drop shape analysis is another widely used way to measure CA [56,57]. In this study, in order to extract CA from the droplet shape obtained by the numerical minimization of the interfacial energies, the dimensionless droplet shape parameter, named the droplet shape quotient Q, was calculated. This parameter and its mean value $\langle Q\rangle$ were defined by the following equations:

$$Q = \frac{S_{\mathrm{d=}}^3}{V^2} \tag{9a}$$

and

$$\langle Q\rangle = \frac{\langle S_{\mathrm{d=}}\rangle^3}{V^2}. \tag{9b}$$

Knowing these values, the corresponding CAs, denoted as θ_{S} and $\langle\theta_{\mathrm{S}}\rangle$, were found from numerical solution of the equation

$$X = 9\pi\frac{(1 + \cos(\theta_{\mathrm{S}}))^3}{(1 - \cos(\theta_{\mathrm{S}}))(2 + \cos(\theta_{\mathrm{S}}))^2} \tag{10}$$

with $X = Q$ or $X = \langle Q\rangle$, respectively.

The calculation of CA based on the use of the droplet shape quotient is a generalization of a number of experimental methods employing direct measurements of geometrical parameters of the droplet: the diameter of curvature of the liquid/gas interface $D = 2R$, the diameter of the droplet base, $d = 2r$ (for CAs greater than 90°) [2] and the droplet height H (H and d are adequate for each CA value) [50], as well as other methods permitting the calculation of the radius of curvature of the free surface of the droplet, R, measured at the projection of the droplet cap on the plane perpendicular to the solid surface [50]. The droplet shape quotient Q is correlated with parameters R, r and H, directly measured from experiment, by the following equations:

$$Q = 9\pi\frac{r^6}{((R+\sqrt{R^2-r^2})(R^2+r^2+R\sqrt{R^2-r^2}))^2} \tag{11}$$

$$Q = 36\pi\frac{r^6}{H^2(H^2 + 3r^2)^2}. \tag{12}$$

The correlations described by eqs. (10)–(12) indicate that the model values of θ_{S} directly correspond to the CAs measured by the experimental methods based on the droplet shape analysis.

3.5 CA of the equivalent droplet

From the simulation results, the Laplace pressure inside the droplet was found and then used for the calculation of the radius of curvature of the droplet free surface, R, [6, 55] and its mean value $\langle R\rangle$, according to the equations

$$R = \frac{2\gamma_{\mathrm{L}}}{\Delta p} \tag{13a}$$

and

$$\langle R\rangle = \frac{2\gamma_{\mathrm{L}}}{\langle\Delta p\rangle}, \tag{13b}$$

where Δp is the pressure difference between inside and outside of the droplet. Equation (13b) defines the average curvature radius of the set of droplets of different locations and hence of different apparent CAs determining the free liquid curvature.

Since in the equilibrium state, the pressure in the whole droplet is the same, the mean curvature at any point of the liquid surface should be identical as a consequence of the Laplace law. However, as shown in fig. 5, the mean curvature C (calculated for all mesh vertices representing the free liquid surface) is not uniform over the whole surface of free liquid. At high elevation, the curvature of free
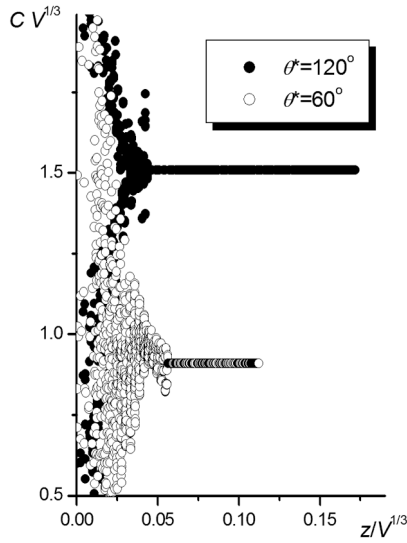
Fig. 5. Dependencies of relative mean curvature C of the liquid surface on the z-coordinate for $\theta^* = 60°$ at $A = 1.5$ and $\theta^* = 120°$ at $A = 0.8$ ($I/V^{1/3} = 0.175$, $L/V^{1/3} = 0.263$, $T/V^{1/3} = 5.8 \cdot 10^{-3}$).

liquid surface is constant and independent of z. At small z, where the liquid surface is corrugated by inhomogeneities, the mean curvature values are widely scattered around the expected value. This dispersion of C values indicates that the Laplace law is violated and the droplet is rather in a metastable state than at equilibrium.

Next, it was assumed that the droplet for which the simulation was performed, existed in equilibrium with another droplet of the same volume but placed on the ideally smooth solid surface (Laplacian droplet). The CAs of this reference thermodynamically equivalent droplet, θ_P, and its mean value $\langle \theta_P \rangle$, were calculated from

$$Y^3 = \frac{3V}{\pi(2 - 3\cos(\theta_P) + \cos^3(\theta_P))} \quad (14)$$

with $Y = R$ or $Y = \langle R \rangle$, respectively.

As far as we know, there is no standard method for estimation of CA based on the idea presented here. Nonetheless, for the purpose of this study the measurability of $\langle \theta_P \rangle$ was assumed.

4 Results and discussion

As explained in the Methodology section, in the course of the optimization process the lattice nodes, determining both the position of the free surface of the droplet and the position of the solid surface, were subjected to random shifts in space at each stage of simulations, in order to mimic the scatter of results due to different initial droplet positions at the surface in repeated trials. As a result of random shifts of nodes of the lattice representing the solid surface, the morphology of this solid surface also underwent small changes and the sizes of inhomogeneities also
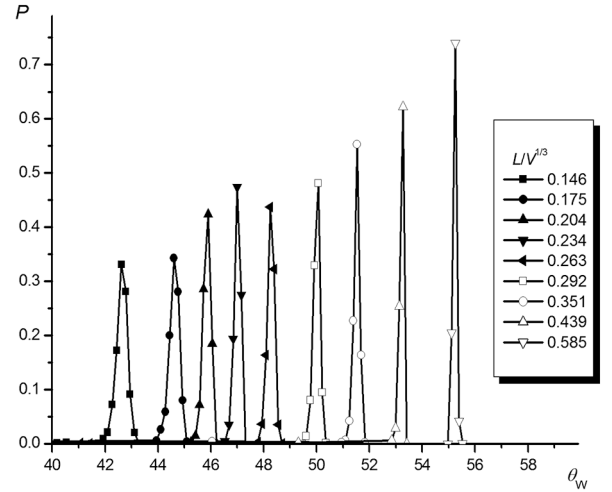

Fig. 6. Distributions of θ_W for different sizes of surface roughness features (L values are indicated in the figure, $I/V^{1/3} = 0.175$, $T/V^{1/3} = 5.8 \cdot 10^{-3}$, $A = 1.5$, $\theta^* = 60°$).

showed a certain scatter. Thus, also the values of Wenzel CA determined on the basis of the surface roughness parameter were somewhat distributed. The distributions of θ_W obtained for different sizes of the surface structure elements, L, and for $\theta^* = 60°$, are presented in fig. 6.

The obtained distributions of θ_W are symmetric and to a high accuracy can be described by the Gaussian distribution with the correlation coefficient of 0.997 ± 0.002. At $\theta^* < 90°$ the value of θ_W monotonically decreases with decreasing L, which is understandable taking into regard that the total area of the surface increases as L decreases. The observed decrease in θ_W is not regular which is a consequence of varying ratio of L to the size of lattice triangles mapping the solid surface. The distributions of θ_W obtained for $\theta^* = 120°$ were analogous to those presented in fig. 6, as they were obtained on the basis of the same simulation results; only the sign of the proportionality coefficient in eq. (6) was changed (*i.e.*, $\cos(\theta^*) = -1/2$). The above presented results characterize the solid surface used in the study and illustrate the predictions following from the Wenzel law. One could expect such dispersion of θ_W values, if its only reason was the deviation of results following from random steps of simulation and there were no systematic biases arising from specific behavior of the droplet.

The θ_E quantifies the free energy of wetting and it was assumed as a reference CA. The obtained values of θ_E are presented in figs. 7 and 8 for $\theta^* = 60°$ and $\theta^* = 120°$, respectively. The θ_E values and their distributions were calculated on the basis of the free energy of wetting, E_d, obtained as a result of the numerical minimization of the total free energy of the system:

$$\frac{S_d}{S_{d=}} = \frac{S_d(\gamma_{SL} - \gamma_S)}{S_{d=}(\gamma_{SL} - \gamma_S)} = \frac{E_d}{E_{d=}}, \quad (15)$$

where $E_{d=}$ is the free energy of wetting of a reference surface, *i.e.* of a smooth solid surface of the area equal to that
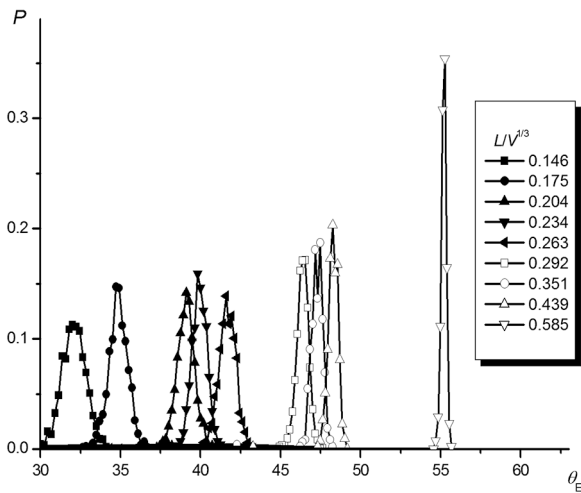
Fig. 7. Distributions of θ_E for different values of L (L values are indicated in the figure, $\theta^* = 60°$, $I/V^{1/3} = 0.175$, $T/V^{1/3} = 5.8 \cdot 10^{-3}$, $A = 1.5$).
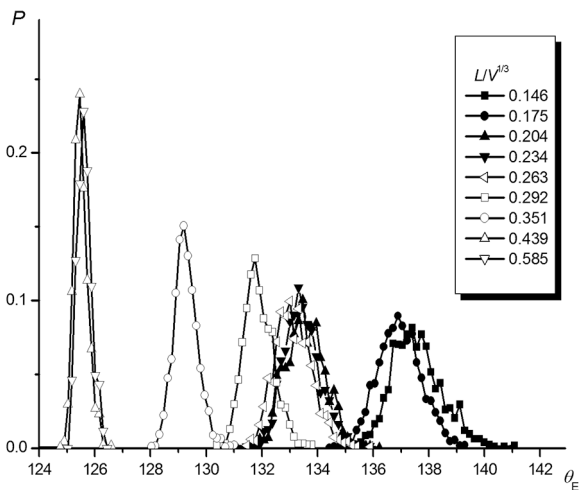

Fig. 8. Distributions of θ_E for different values of L (L values are given in the figure, $\theta^* = 120°$, $I/V^{1/3} = 0.175$, $T/V^{1/3} = 5.8 \cdot 10^{-3}$, $A = 1.0$).

Fig. 9. Distributions of θ_T, θ_S and θ_P for different values of L (L values are given in the figure, $\theta^* = 60°$, $I/V^{1/3} = 0.175$, $T/V^{1/3} = 5.8 \cdot 10^{-3}$, $A = 1.5$).

of projected area, while γ_{SL} and γ_S denote solid-liquid and solid-vapor interfacial tensions, respectively. Thus, the values of θ_E hold the information on the real values of interfacial energy of the system.

As shown in fig. 7, the distributions of θ_E, similarly as those of θ_W, decrease monotonically with decreasing L. However, in this case the dependence is more complicated. Some individual distributions are shifted to make groups of two or three, they are broader, especially for small L, and some of them (at $L/V^{1/3} = 0.146$, 0.263, 0.351 and 0.439) reveal a hyperfine structure indicating that a given total distribution is a sum of a few distributions with the expected values of θ_E differing by 1° to 3°. The changes in the distributions follow from the fact that some of the possible final shapes of the droplet are preferred because of the pinning effect. As a result of this effect, in the course
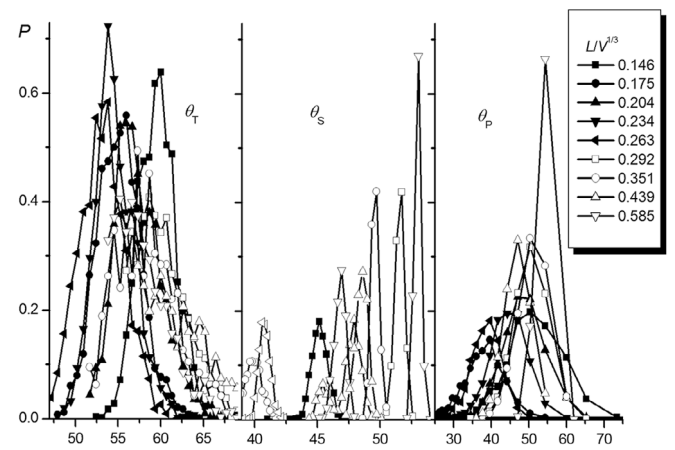
of the rearrangement of the droplet shape from its initial to final form, the triple line shifts from the solid surface structure elements, on which it can freely move and the inclination of free liquid surface is invariably θ^*, to the elements on which the position of the contact line is strictly defined by sharp edges but the inclination of liquid surface can vary and must satisfy inequality (5). The scatter of θ_E for a given L implies that the modeled droplet can assume many different morphologies, differing, *e.g.*, in the degree of anisotropy and in the mean radius of curvature of the droplet free surface, in the regions near the edge at which the triple line is pinned. It means that the morphologies, in general, do not correspond to the state of thermodynamic equilibrium of the droplet but only to the stationary states at local energy minima at which the Laplace law is not satisfied (see fig. 5). For $\theta^* = 120°$ (fig. 8), θ_E values behave analogously, but with more pronounced broadening and hyperfine structures.

Figure 9 presents the distributions of θ_T, θ_S and θ_P for different values of L. These distributions are generally much broader than those of θ_E (particularly for θ_T and θ_P). They are also disordered in the sense that the sequences of maxima in the distributions are different from those of θ_E and θ_W, which is best visible for θ_S. It is difficult to find any correlation between the distributions shown in fig. 9 and those of θ_E and θ_W.

The above-presented results were obtained at the same values of parameters T and A, which in the simulations mimic different locations of the droplet in respect to the surface structure elements in repeated trials of the CA measurement and the impact of the droplet on the surface, respectively.

The influence of the amplitude of fluctuations, T, on the mean values of CAs estimated by different methods is illustrated in fig. 10. As seen, the mean CA values are practically independent of T in the range considered in this study (the simulations were performed for $T/V^{1/3}$ of $5.8 \cdot 10^{-3}$ and $5.8 \cdot 10^{-2}$). Hence, the influence of this parameter on the simulation results can be neglected. However,
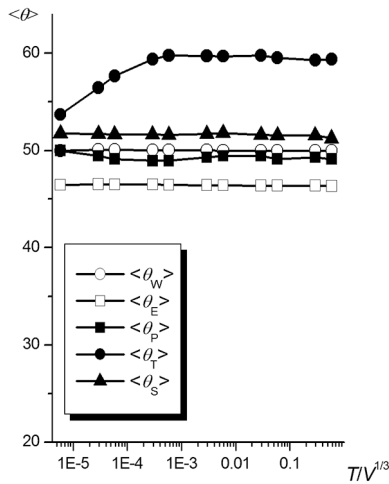
Fig. 10. Dependencies of $\langle\theta_W\rangle$, $\langle\theta_E\rangle$, $\langle\theta_P\rangle$, $\langle\theta_T\rangle$ and $\langle\theta_S\rangle$ against T ($\theta^* = 60°$, $A = 1.5$).
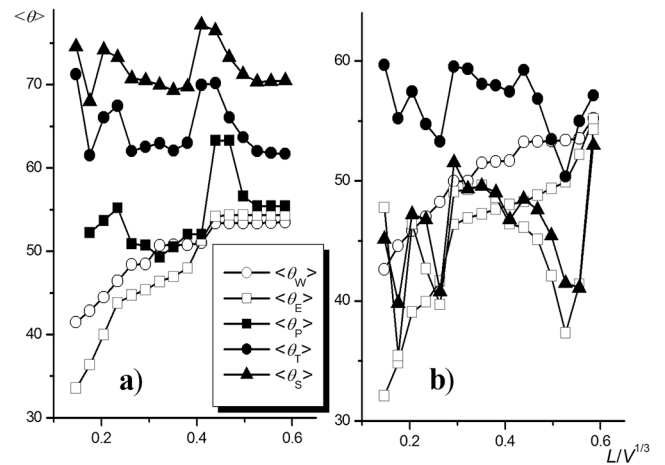

Fig. 11. The influence of A on the CA values estimated by different approaches as identified in the figure legend, $I/V^{1/3} = 0.175$, $L/V^{1/3} = 0.263$, $T/V^{1/3} = 5.8 \cdot 10^{-3}$ and a) $\theta^* = 60°$, $A_0 = 1.732$, b) $\theta^* = 120°$, $A_0 = 0.577$.

one should be aware that although the T value does not influence the simulation results, the fluctuations defined by T are the only factor responsible for the appearance of different morphologies of the droplets, imitating the random character of the droplet morphology on the solid surface and the randomness of the results of the CA measurements.

In the simulations, the droplet was initialized as a cuboid, whose shape was determined by the parameter A. As follows from the comparison of results presented in figs. 11a and b, there is no distinct influence of A on the values of $\langle\theta_W\rangle$, for both studied values of θ^*. In the whole A range studied, the values of $\langle\theta_W\rangle$ underestimate the effect of surface roughness on CA both for $\theta^* = 60°$ and for $\theta^* = 120°$ (being too high or too low, respectively), but they are more similar to corresponding $\langle\theta_E\rangle$ values then the estimations of CAs obtained from simulated experimental measurements. Moreover, at $\theta^* = 60°$

Fig. 12. The influence of L on the CA values estimated by different approaches (identified in the figure legend) for $I/V^{1/3} = 0.175$, $T/V^{1/3} = 5.8 \cdot 10^{-3}$, $\theta^* = 60°$ and a) $A = 0.6$, b) $A = 1.5$.
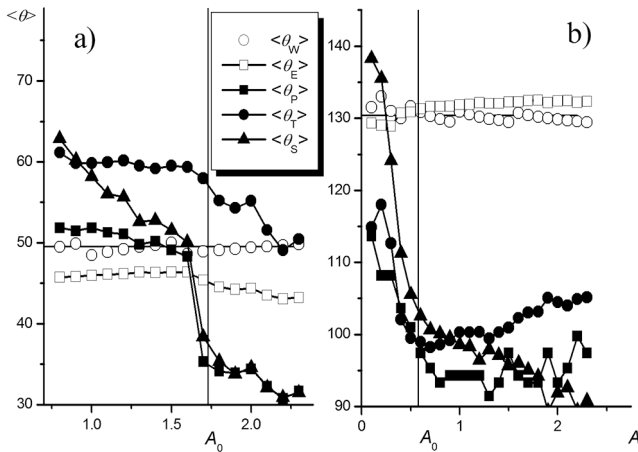
a noticeable change in $\langle\theta_E\rangle$ is observed in the vicinity of a certain value of A (denoted as A_0), which corresponds to the d/H ratio characterizing the shape of the droplet at equilibrium. For higher A values the pinning of the triple line of the flattened droplet to surface defects hinders the rearrangement of the droplet to its equilibrium shape and, in consequence, the difference between $\langle\theta_E\rangle$ and $\langle\theta_W\rangle$ is greater. It is noteworthy that at $\theta^* = 120°$, for which the triple line is relatively short, and hence, the contribution of the pinning phenomenon is smaller, the Wenzel equation gives quite good estimation of $\langle\theta_E\rangle$.

On the other hand, a significant dependence of the values of $\langle\theta_P\rangle$ and $\langle\theta_S\rangle$ on A is found. Moreover, it can be also observed that when A tends to a certain value slightly smaller than A_0, the values of these CAs approach those of $\langle\theta_E\rangle$. The exception is the behavior of $\langle\theta_P\rangle$ for $\theta^* = 120°$; in the studied A range the value of $\langle\theta_P\rangle$ does not reach that of $\langle\theta_E\rangle$. The values of $\langle\theta_T\rangle$, which are the most sensitive to the conditions at the triple line from among CA estimations employed in the study, differ considerably from those of $\langle\theta_E\rangle$ in almost whole A range examined.

A deviation of $\langle\theta_P\rangle$ from the expected value $\langle\theta_E\rangle$ is caused by the fact that the rearrangement of the droplet shape toward that of a spherical cup is hindered by the pinning effect (as seen in figs. 1b and c, the triple line is contorted). With this arrested droplet shape, the system does not satisfy the Plateau law. So, the measured values of CAs are not the equilibrium values predicted by the Wenzel law.

Figures 12 and 13 summarize the results of estimation of CA by means of the approaches described in sect. 3, in the form of plots of $\langle\theta_W\rangle$, $\langle\theta_E\rangle$, $\langle\theta_P\rangle$, $\langle\theta_T\rangle$ and $\langle\theta_S\rangle$ against L. According to fig. 12a, representing the results found for $\theta^* = 60°$ and A value small as compared to A_0 ($A = 0.6$), the CA estimations based both on the Wenzel law as well as on simulated experimental measurements give higher values than the corresponding values of $\langle\theta_E\rangle$ in the whole
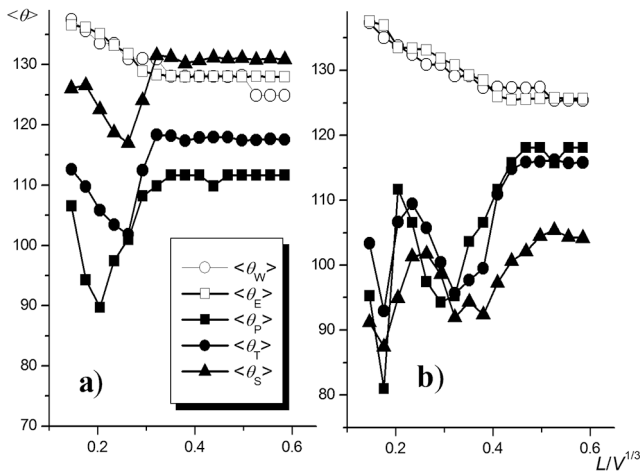
Fig. 13. The influence of L on the CA values estimated by different approaches (identified in the figure legend) for $I/V^{1/3} = 0.175$, $T/V^{1/3} = 5.8 \cdot 10^{-3}$, $\theta^* = 120°$ and a) $A = 0.3$, b) $A = 1.0$.

L range studied. On the other hand, when the initial droplet shape is only weakly distorted (fig. 12b), the estimations based on simulated measurements, at least $\langle \theta_P \rangle$ and $\langle \theta_S \rangle$ are closer to the corresponding values of $\langle \theta_E \rangle$, but their scattering is greater than the error of any standard experimental methods of CA measurement [50]. The $\langle \theta_T \rangle$ estimations differ considerably from the expected $\langle \theta_E \rangle$ values for both A studied. These differences are greater than the error reported for the techniques of CA determinations based on direct measurement of the tangent angle at the three-phase contact line (*e.g.* 5% in the tilting plate method [2]).

For $\theta^* = 120°$ (fig. 13), at which the contribution of the effect of corrugation of triple line becomes less severe (because of smaller length of the triple line), the agreement between $\langle \theta_W \rangle$ and $\langle \theta_E \rangle$ was obtained at both selected values of parameter A (0.3 and 1.0). However, the results of simulated experimental measurements deviate significantly from the $\langle \theta_E \rangle$ values; except for some estimations of $\langle \theta_S \rangle$ obtained for the value of A parameter corresponding to only a small deviation of the initial droplet shape from the hypothetical equilibrium shape.

The distinct differences in CAs estimated by various approaches, as presented in figs. 12 and 13, indicate that the apparent CA cannot be used as a measure of the solid-surface free energy if the roughness scale of the solid is not small enough.

5 Conclusions

In this paper different approaches to the assessment of the CA values from numerical simulations of a liquid droplet settled on surfaces with meso-scale roughness pattern were employed and the obtained results were analyzed in terms of the applicability of the Wenzel law for the determination of the solid-surface free energy.

It was found that the Wenzel equation overestimates (for $\theta^* = 60°$) or underestimates (for $\theta^* = 120°$) the values of apparent CA as compared to those estimated on the basis of correctly calculated free energy of wetting, that is, when the actual solid surface occupied by the droplet, not the surface roughness parameter, is taken into account.

It was also found that the CA values obtained from simulated experimental measurements, *i.e.*, $\langle \theta_T \rangle$, $\langle \theta_S \rangle$ and $\langle \theta_P \rangle$, do not provide a correct description of the thermodynamics of a droplet deposited on a rough solid surface, since, in general, there is no direct correlation between these CAs and the free energy of wetting. The differences between these "measured" CAs and the CA values estimated on the basis of the free energy of wetting ($\langle \theta_E \rangle$), increase with increasing deviation of the initial droplet shape from the equilibrium shape ($|A - A_0|$). This relation follows from the dependence of the resulting morphology of the droplet on the mode of its deposition on the solid surface.

A droplet deposited on the solid surface with the meso-scale roughness can exist in a metastable state for which the Laplace law is not satisfied, *i.e.* the curvature of the free liquid surface is not uniform and exhibits significant dispersion close to the triple line. It is so because the values of actual CAs are not the same at different surface structure elements, and hence, there are variations in the slope of the tangent to the local free liquid surface of the droplet.

The discrepancies between CA estimations yielded by different approaches result from the phenomena taking place at the triple line. In the range of θ^* studied, the corrugation of the triple line is caused by the pinning effect. In a wider range of θ^* other effects, related to the Concus-Finn condition, are expected (3).

Author contribution statement

All authors contributed equally to the paper.

References

1. M. Rauscher, S. Dietrich, Annu. Rev. Mater. Res. **38**, 143 (2008).
2. Y. Yuan, T.R. Lee, in *Surface Science Techniques*, edited by G. Bracco, B. Horst, Springer Ser. Surf. Sci., Vol.**51** (Springer-Verlag, Berlin, Heidelberg, 2013).

3. T.T Chau, W.J. Bouckard, P.T. Koh, A.V. Nguyen, Adv. Colloid Interface Sci. **150**, 106 (2009).
4. Y. Zhao, Q. Lu, M. Li, X. Li, Langmuir **23**, 6212 (2007).
5. T. Young, Philos. Trans. R. Soc. London **95**, 65 (1805).
6. R.N. Wenzel, Ind. Eng. Chem. **28**, 988 (1936).
7. A.B.D. Cassie, S. Baxter, Trans. Faraday Soc. **40**, 546 (1944).
8. A. Promraksa, L.-J. Chen, J. Colloid Interface Sci. **384**, 172 (2012).
9. J. Berthier, K.A. Brakke, *The Physics of Microdroplets* (John Wiley & Sons, Inc. Hoboken, New Jersey, 2012).
10. P.-G. de Gennes, F. Brochard-Wyart, D. Quere, *Capillarity and Wetting Phenomena: Drops, Bubbles, Pearls, Waves* (Springer Science+Business Media, New York, 2004).
11. G. McHale, S.J. Elliott, M.I. Newton, N.J. Shirtcliffe, in *Contact Angle, Wettability and Adhesion*, Vol. **6**, edited by K.L. Mittal (CRC Press, Boca Raton, 2009).
12. M. Flemming, L. Coriand, A. Duparré, in *Superhydrophobic Surfaces*, edited by A. Carré, K.L. Mittal (CRC Press, Boca Raton, 2009).
13. R. Shuttleworth, G.L.J. Bailey, Discuss. Faraday Soc. **3**, 16 (1948).
14. A. Marmur, in *Contact Angle, Wettability and Adhesion*, Vol. **6**, edited by K.L. Mittal (CRC Press, Boca Raton, 2009).
15. P.S. Swain, R. Lipowsky, Langmuir **14**, 6772 (1998).
16. G. Wolansky, A. Marmur, Colloids Surf. **156**, 381 (1999).
17. C. Dorrer, J. Rühe, Langmuir **24**, 1959 (2008).
18. T. Cubaud, M. Fermiger, Europhys. Lett. **55**, 239 (2001).
19. L. Courbin, E. Denieul, E. Dressaire, M. Roper, A. Ajdari, H.A. Stone, Nat. Mater. **6**, 661 (2007).
20. C. Dorrer, J. Rühe, Langmuir **23**, 3179 (2007).
21. H. Kusumaatmaja, R.J. Vrancken, C.W.M. Bastiaanses, J.M. Yeomans, Langmuir **24**, 7299 (2008).
22. G. Wolansky, A. Marmur, Langmuir **14**, 5292 (1998).
23. S. Brandon, N. Haimovich, E. Yeger, A Marmur, J. Colloid Interface Sci. **263**, 237 (2003).
24. E.Yu. Bormashenko, *Wetting of Real Surfaces. De Gruyter Studies in Mathematical Physics* (De Gruyter, Berlin, 2013).
25. G. McHale, Langmuir **23**, 8200 (2007).
26. L. Gao, T.J. McCarthy, Langmuir **23**, 3762 (2007).
27. H.Y. Erbil, C.E. Cansoy, Langmuir **25**, 14135 (2009).
28. P.G. de Gennes, Rev. Mod. Phys. **57**, 827 (1985).
29. A. Checco, H. Schollmeyer, J. Daillant, P. Guenoun, Langmuir **22**, 116 (2006).
30. H.Y. Erbil, Surf. Sci. Rep. **69**, 325 (2014).
31. J. Drelich, E. Chibowski, D.D. Meng, K. Terpilowski, Soft Matter **7**, 9804 (2011).
32. A. Promraksa, Y.-C. Chuang, L.-J. Chen, J. Colloid Interface Sci. **418**, 4 (2014).
33. M. Miva, A. Nakajima, A. Fujishima, K. Hashimoto, K. Watanabe, Langmuir **16**, 5754 (2000).
34. A. Marmur, Langmuir **19**, 8343 (2003).
35. J. Bico, U. Thiele, D. Quéré, Colloids Surf. A **206**, 41 (2002).
36. E. Raphaël, P.G. de Gennes, J. Chem. Phys. **90**, 7577 (1989).
37. L. Leger, J.F. Joanny, Rep. Prog. Phys. **55**, 431 (1992).
38. J.F. Joanny, P.G. de Gennes, J. Chem. Phys. **81**, 552 (1984).
39. J.A. Marsh, A. Cazabar, Europhys. Lett. **23**, 45 (1993).
40. G.D. Nadkarni, S. Garoff, Europhys. Lett. **20**, 523 (1992).
41. R.H. Detree, R.E. Johnson, Adv. Chem. Ser. **43**, 112 (1964).
42. R.H. Detree, R.E. Johnson, Adv. Chem. Ser. **43**, 136 (1964).
43. R.H. Detree, R.E. Johnson, J. Phys. Chem. **68**, 1744 (1964).
44. P.S.H. Forsberg, C. Pries, M. Brinkmann, R. Sedev, J. Ralson, Langmuir **26**, 860 (2010).
45. J.B. Boreyko, C.P. Collier, J. Phys. Chem. **117**, 18084 (2013).
46. S.-H. Choi, B.-M.Z. Newby, Langmuir **19**, 7427 (2003).
47. M. Hans, F. Müller, S. Grandthyll, S. Hüfner, F. Mücklich, Appl. Surf. Sci. **263**, 416 (2012).
48. B. Bhushan, Y.C. Jung, M. Nosonovsky, in *Springer Handbook of Nanotechnology*, edited by B. Bhushan (Springer, Berlin, Heidelberg, 2001) pp. 1437–1524.
49. P. Concus, R. Finn, Proc. Natl. Am. Sci. **63**, 292 (1969).
50. D. Langbein, *Capillary Surfaces: Shape–Stability–Dynamics, in Particular Under Weightlessness* (Springer-Verlag, Berlin, Heidelberg, 2002).
51. K.A. Brakke, Exp. Math. **1**, 141 (1992).
52. K.A. Brakke, Surface Evolver Manual, Version 2.70, 2014, http://www.susqu.edu/brakke/evolver/html/evolver.htm.
53. S.F. Lunkad, V.V. Buwa, K.D.P. Nigam, Chem. Eng. Sci. **62**, 7214 (2007).
54. A.L. Yarin, Annu. Rev. Fluid Mech. **38**, 159 (2006).
55. Scilab Manual, http://help.scilab.org/docs/5.5.1/en_US/index.html.
56. M. Guilizzoni, J. Colloid Interface Sci. **364**, 230 (2011).
57. M. Hoorfar, A.W. Neumann, Adv. Colloid Interface Sci. **121**, 25 (2006).